

Coherent FDA Radar Systems: Joint Design of Transmitting and Receiving Array Weighters

Wenkai Jia, Wen-Qin Wang, *Senior Member, IEEE*, Shungsheng Zhang

Abstract—Due to the frequency offset across its array elements, frequency diverse array (FDA) will generate angle-range-dependent and time-variant transmit beampattern. Since existing investigations usually focus on FDA transmitter and only instantaneous beampattern is considered, which cannot fully exploit the time-range characteristics of FDA radar for enhanced performance, in this paper we formulate a multi-carrier mixing receiver for coherent pulsed-Doppler FDA radar to effectively retain the range information of FDA radar returned signals in subsequent receiver processing. Accordingly, the joint transmitter and receiver is systematically modeled with time-range relationship consideration. More importantly, we optimally design the joint transmitting and receiving weighters by maximizing the radiated energy within the desired range-angle sections for given total energy. All proposed methods are verified by simulation results.

Index Terms—Frequency diverse array (FDA), coherent FDA radar, range-time relationship, range-dependent, transceiver design, joint transmitter-receiver optimization.

I. INTRODUCTION

The architecture of multiple transmitters and receivers enables the multiple-input multiple-output (MIMO) radar [1] superiority to phased-array radar in parameter identifiability [2] and target detection [3]. Nevertheless, the beam steering of MIMO radar is fixed in an angle for all ranges. This range-independent directivity may limit its applications, such as joint range and angle estimation, range ambiguous clutter suppression and range-dependent interference mitigation.

Unlike the MIMO radar with a single carrier frequency, frequency diverse array (FDA) adds small frequency offsets (FOs) across the array elements to provide potentials for range-dependent energy management and support many promising applications [4]–[6]. To achieve the desired beampattern in the range-angle plane, a FDA transmit beamspace matrix optimization method based on alternating direction method of multipliers (ADMM) was proposed in [7]. In [8], cognitive FDA with situational awareness was introduced to avoid undesired strong interferences. And for three-dimensional target localization, [9] proposed an adaptive range-angle-Doppler processing approach by exploiting the increased degree of

freedoms (DoFs) in transmit, receive, and pulse dimensions in FDA. Particularly, an adaptive FDA transmit power allocation scheme was designed for spectral interference avoidance through maximizing the output signal-to-interference-plus-noise ratio (SINR) in [10], which shows that FDA radar is able to suppress mainlobe spectral interferences. Moreover, [11] investigated the low probability of intercept (LPI) properties of FDA transmitted signals under typical passive reconnaissance techniques.

However, the aforementioned studies did not consider the range-time relationship because they only consider instantaneous time. In addition, current FDA research mostly focuses on the design and application of FDA transmitters, while optimal FDA receiver design is rarely published. In fact, FDA produces time-variant or self-scanning transmit beampattern, which range dependency depends on how to effectively receive the FDA returns. The multi-channel matched filtering receiver structure for a pulsed-FDA radar was designed in [12], which can handle both non-overlapping and overlapping FDA signals, but the range-time relationship is still ignored and how to retain the range-related steering vector is not clearly discussed.

Xu *et al.* investigated FDA equivalent transmit beamforming at the receiver, and applied a series of filters and mixers [13] or symmetrical logarithmic FOs [14] to deal with the time-variant FDA transmit beampattern. However, they only designed the receive weightier, but the transmit weightier was not investigated. More seriously, the beamforming performance will degrade significantly in some scenarios if uncontrolled transmit power distribution is adopted. An intuitive method is to jointly optimize the transmitting and receiving weighters via power maximization strategy. The transmitting FDA weightier and receiving phased-array weightier can jointly optimized to focus the beamforming position in range-angle plane. To our knowledge, joint design of FDA transmitter and receiver was not discussed in open literature.

Different from existing FDA literature, this paper systematically reformulates the FDA transmit signal model with time-range relationship consideration. Then, considering a coherent pulse-Doppler radar, we explain why the received FDA signal can retain the range information of a target. Accordingly, we design the optimal FDA receiver based on the maximum likelihood criterion. Then, we optimize the joint transmit and receive weighting vectors for a coherent FDA radar by maximizing the energy radiated within the desired range-angle sections.

In summary, our main contributions are highlighted as follows:

- 1) Time-range relationship is a fundamental problem in FDA

This work was supported by National Natural Science Foundation of China under grant 62171092 (Corresponding author: Wen-Qin Wang).

W.K. Jia and W.-Q. Wang are with School of Information and Communication Engineering, University of Electronic Science and Technology of China, Chengdu, 611731, P. R. China. (email: mrwenkaij@126.com; wqwang@uestc.edu.cn). W.-Q. Wang also is with the Yangtze Delta Region Institute (Huzhou), University of Electronic Science and Technology of China, Huzhou, 313001, China. S.S. Zhang is with the Research Institute of Electronic Science and Technology, University of Electronic Science and Technology of China, Chengdu, 611731, China (e-mail: zhangss@uestc.edu.cn).

signal modeling, but it is not well handled in existing studies by only considering instantaneous time [12], [15], [16]. In this paper, we reformulate the FDA transmitted signal model and the corresponding FDA integral transmit beampattern is derived with time-range relationship consideration.

- 2) The range-related steering vector plays a vital role in FDA radar applications [17], [18], which is the essence of FDA compared with conventional MIMO and phased-array radars [5], [12], [19]. But why the range-related steering vector can be retained in the received FDA signal is still not clearly explained in the literature. Considering a coherent pulse-Doppler radar, we analyze the difference between single-carrier mixing and multi-carrier mixing for FDA radar and verify that only the multi-carrier mixing can retain the range-related steering vector in received FDA signal.
- 3) We design the optimal FDA receiver structure from the perspective of maximum likelihood estimation and sufficient statistics [20] with considering the time-range relationship.
- 4) Considering the derived FDA integral transmit beampattern, we optimize the joint transmit and receive weighting vectors for a coherent FDA radar by maximizing the energy radiated within the desired range-angle sections, together with taking into account a similarity constraint between the designed transmit weight and the reference weight. Moreover, an iterative algorithm is developed to deal with this non-convex optimization problem.

The remaining sections are organized as follows. In Section II, the time-range relationship of FDA signal model is discussed and the reason of range-related steering vector retention is explained, followed by the optimal FDA receiver structure. Next, Section III optimizes the joint transmitting and receiving array weighters optimization problem. Finally, Section IV provides simulation results to verify all theoretical analysis and conclusions are drawn in Section V.

Notations: Lower case letters \mathbf{a} and upper case letters \mathbf{A} , respectively, represent vectors and matrices. Conjugate, transpose and conjugate transpose operators are denoted by the symbols $(\cdot)^c$, $(\cdot)^T$ and $(\cdot)^H$, respectively. For a matrix \mathbf{A} , we use $\mathbf{A}(i, j)$ as the (i, j) th element of \mathbf{A} , $\text{vec}\{\mathbf{A}\}$ as the column vector of \mathbf{A} , $\text{Tr}\{\mathbf{A}\}$ as the trace of \mathbf{A} , $\text{Rank}\{\mathbf{A}\}$ as the rank of \mathbf{A} and $\lambda_{\max, \text{vec}}\{\mathbf{A}\}$ as the principal eigenvector of \mathbf{A} . The symbol $\text{diag}\{\mathbf{a}\}$ denotes the diagonal matrix with the diagonal entries formed by \mathbf{a} and $\|\mathbf{a}\|$ denotes the Euclidean norm of \mathbf{a} . \mathbf{I}_M and $\mathbf{1}_M$ represent the identity matrix and all-ones matrix with size $M \times M$, respectively. $|\cdot|$ is the absolute value, $*$ is the convolution operator and $\mathbb{E}\{\cdot\}$ is the statistical expectation of a random variable. The sets of $M \times M$ complex-valued (real-valued) matrices are defined as $\mathbb{C}^{M \times M}$ ($\mathbb{R}^{M \times M}$) and $\mathbb{C}^{M \times M} \cap \mathbb{R}^{M \times M}$ means that the intersection of $\mathbb{C}^{M \times M}$ and $\mathbb{R}^{M \times M}$. We let $\succ=$ stand for generalized matrix inequality, and Hadamard matrix product and Kronecker matrix product are expressed as \odot and \otimes , respectively.

II. SIGNAL MODEL

A. FDA Transmit Signal Model

Consider a standard pulsed-FDA radar system with M transmit antennas [21]. The first transmitted pulse via the m th element is

$$\phi_m(t) = w_{T,m}^c \text{rect}\left(\frac{t}{T_p}\right) s(t) e^{j2\pi f_m t}, \quad m = 1, 2, \dots, M, \quad (1)$$

where $w_{T,m}$ is the corresponding transmit weight, $\text{rect}\left(\frac{t}{T_p}\right) s(t) = \begin{cases} s(t), & t \in [0, T_p] \\ 0, & t \in [0, T_{PRT}] \end{cases}$ represents the baseband complex waveform with unit energy, namely, $\int_{T_p} s(t) s^c(t) dt = 1$, where T_p and T_{PRT} denote the pulse duration and pulse repetition time, respectively, and $f_m = f_c + (m-1)\Delta f$ is the carrier frequency for the m th element with Δf being the frequency offset.

Under the narrowband assumption $\frac{Md}{c} \ll \frac{1}{B_s(t)}$ with $B_s(t)$ being the bandwidth of the baseband complex waveform $\text{rect}\left(\frac{t}{T_p}\right) s(t)$, the synthesized signal at the target location with a range-angle pair (r, θ) can be expressed as

$$\begin{aligned} r_T(t) &= \sum_{m=1}^M \phi_m\left(t - \frac{r_m}{c}\right) \\ &\approx \sum_{m=1}^M w_{t,m}^c \text{rect}\left(\frac{t - r/c}{T_p}\right) s\left(t - \frac{r}{c}\right) e^{j2\pi f_m(t - \frac{r_m}{c})} \end{aligned} \quad (2)$$

where $r_m = r - (m-1)d \sin \theta$ denotes the slant range from the m th element to the target with d being the inter-element spacing and c the speed of light. Taking the first element as the reference, (2) can be simplified into

$$\begin{aligned} r_T(t) &= \text{rect}\left(\frac{t - r/c}{T_p}\right) s\left(t - \frac{r}{c}\right) e^{j2\pi f_c(t - \frac{r}{c})} \\ &\quad \cdot \mathbf{w}^H [\mathbf{e}(t) \odot \mathbf{a}_{T,r}(r) \odot \mathbf{a}_{T,\theta}(\Delta f, \theta)] \end{aligned} \quad (3)$$

where

$$\begin{aligned} \mathbf{e}(t) &= [1, e^{j2\pi \Delta f t}, \dots, e^{j2\pi (M-1) \Delta f t}]^T, \\ \mathbf{a}_{T,\theta}(\Delta f, \theta) &= [1, e^{j2\pi d \frac{\sin \theta}{c} (f_c + \Delta f)}, \dots, e^{j2\pi d \frac{\sin \theta}{c} [(M-1)f_c + (M-1)^2 \Delta f]}]^T, \\ \mathbf{a}_{T,r}(r) &= [1, e^{-j2\pi \Delta f \frac{r}{c}}, \dots, e^{-j2\pi (M-1) \Delta f \frac{r}{c}}]^T. \end{aligned} \quad (4)$$

In [12], [22], the FDA transmit beampattern is written as

$$P(t, \theta, r) = |\mathbf{w}^H [\mathbf{e}(t) \odot \mathbf{a}_{T,r}(r) \odot \mathbf{a}_{T,\theta}(\Delta f, \theta)]|^2. \quad (5)$$

However, note that the time variable t has a direct relation with range r in (3) and consequently, Eq. (5) is inaccurate to ignore the time variable t in FDA transmit beampattern. It should be modified into

$$\begin{aligned} P(t, \theta, r) &= \left| \mathbf{w}^H \left[\left(\text{rect}\left(\frac{t - r/c}{T_p}\right) \mathbf{e}(t) \right) \odot \mathbf{a}_{T,r}(r) \odot \mathbf{a}_{T,\theta}(\Delta f, \theta) \right] \right|^2 \\ &= P_{\text{new}}(t, \theta) = |\mathbf{w}^H [\mathbf{e}(t) \odot \mathbf{a}_{T,\theta}(\Delta f, \theta)]|^2. \end{aligned} \quad (6)$$

B. FDA Range-Related Steering Vector Analysis

Consider the pulsed-FDA radar with N receive antennas. According to (2), the returned pulse reflected from the far-filid target to the n th receive antenna can be written as

$$\begin{aligned} \bar{r}_{R,n}(t) = & \varsigma(r, \theta) e^{j2\pi(n-1)d \sin \theta \frac{f_c}{c}} \\ & \cdot \text{rect}\left(\frac{t - 2r/c}{T_p}\right) s\left(t - \frac{2r}{c}\right) e^{j2\pi f_c(t - \frac{2r}{c})} \\ & \cdot \sum_{m=1}^M \left\{ w_{T,m}^c e^{j2\pi(m-1)\Delta f(t - \frac{2r}{c})} \right. \\ & \cdot \left. e^{j2\pi d \frac{\sin \theta}{c} [(m-1)f_c + (m-1)^2 \Delta f]} \right\} \end{aligned} \quad (7)$$

$, n = 1, 2, \dots, N.$

where $\varsigma(r, \theta)$ is the complex amplitudes proportional to radar cross section (RCS) of the target.

According to the pulse-Doppler radar mechanism [23], we define the range sampling gate as

$$\text{rect}_g\left(\frac{t - 2r_{g,\min}/c}{T_g}\right) = \begin{cases} 1, & t \in \left[\frac{2r_{g,\min}}{c}, \frac{2r_{g,\min}}{c} + T_g\right] \\ 0, & \text{others} \end{cases} \quad (8)$$

where $r_{g,\min}$ is the minimum range of interest and $T_g = \frac{2r_{g,\max}}{c} - \frac{2r_{g,\min}}{c}$ represents the radar range gate with $\frac{2r_{g,\max}}{c}$ being the maximum range of interest. Then, the effective signal returned to the n th receive antenna can be expressed as

$$\begin{aligned} r_{R,n}(t) = & \varsigma(r, \theta) e^{j2\pi f_c(t - \frac{2r}{c})} e^{j2\pi(n-1)d \sin \theta \frac{f_c}{c}} \\ & \cdot \text{rect}_g\left(\frac{t - 2r_{g,\min}/c}{T_g}\right) \text{rect}\left(\frac{t - 2r/c}{T_p}\right) s\left(t - \frac{r}{c}\right) \\ & \cdot \sum_m \left\{ w_{T,m}^c e^{j2\pi(m-1)\Delta f(t - \frac{2r}{c})} \right. \\ & \cdot \left. e^{j2\pi d \frac{\sin \theta}{c} [(m-1)f_c + (m-1)^2 \Delta f]} \right\} \end{aligned} \quad (9)$$

$, n = 1, 2, \dots, N.$

Fig. 1 illustrates the coherent pulse-Doppler FDA radar operation and sampling schemes. The first, the second and the third rows represent the returned signal, local waveform and acquired signals mixing with local waveform, respectively. We make two assumptions:

- 1) Different transmitted pulses have the same initial carrier phase, which initial phase is denoted by φ_a .
- 2) Different received pulses also have the same initial phase for all local carriers.

Then, from (7), the phase of the first FDA pulse at Point 1 in Fig. 1 is

$$\begin{aligned} & \sum_{m=1}^M \left\{ w_{T,m}^c e^{j2\pi(m-1)\Delta f(t - \frac{2r}{c}) + j\varphi_a} \right\} \Big|_{t=\frac{2r}{c}} \\ & = e^{j\varphi_a} \sum_{m=1}^M w_{T,m}^c e^{j2\pi d \frac{\sin \theta}{c} [(m-1)f_c + (m-1)^2 \Delta f]} \end{aligned} \quad (10)$$

For local single carrier f_c , the phase at Point 4 is

$$e^{j2\pi f_c(t - \frac{2r_{b,\min}}{c}) + \varphi_b} \Big|_{t=\frac{2r}{c}} = e^{j2\pi f_c(\frac{2r}{c} - \frac{2r_{b,\min}}{c})} e^{j\varphi_b} \quad (11)$$

But, for local multi-carrier $f_c + (m' - 1)\Delta f$, $m' = 1, 2, \dots, M$, the phase at Point 4 for the m' th carrier should be

$$\begin{aligned} & e^{j2\pi[f_c + (m'-1)\Delta f](t - \frac{2r_{b,\min}}{c}) + \varphi_b} \Big|_{t=\frac{2r}{c}} \\ & = e^{j2\pi[f_c + (m'-1)\Delta f](\frac{2r}{c} - \frac{2r_{b,\min}}{c})} e^{j\varphi_b}. \end{aligned} \quad (12)$$

Next, after carrier demodulation operation, the phase of the first FDA pulse at Point 8 for local single-carrier and multi-carrier can be obtained, respectively, as

$$\begin{aligned} & e^{j\varphi_a} \sum_{m=1}^M w_{T,m}^c e^{j2\pi d \frac{\sin \theta}{c} [(m-1)f_c + (m-1)^2 \Delta f]} \\ & \cdot \left[e^{j2\pi f_c(\frac{2r}{c} - \frac{2r_{b,\min}}{c})} e^{j\varphi_b} \right]^c \\ & = \left[e^{-j2\pi f_c(\frac{2r}{c} - \frac{2r_{b,\min}}{c})} e^{j(\varphi_a - \varphi_b)} \right] \end{aligned} \quad (13)$$

$$\begin{aligned} & \cdot \sum_{m=1}^M w_{T,m}^c e^{j2\pi d \frac{\sin \theta}{c} [(m-1)f_c + (m-1)^2 \Delta f]} \\ & e^{j\varphi_a} \sum_{m=1}^M w_{T,m}^c e^{j2\pi d \frac{\sin \theta}{c} [(m-1)f_c + (m-1)^2 \Delta f]} \\ & \cdot \left[e^{j2\pi[f_c + (m'-1)\Delta f](\frac{2r}{c} - \frac{2r_{b,\min}}{c})} e^{j\varphi_b} \right]^c \\ & = e^{-j2\pi(m'-1)\Delta f(\frac{2r}{c} - \frac{2r_{b,\min}}{c})} \\ & \cdot e^{-j2\pi f_c(\frac{2r}{c} - \frac{2r_{b,\min}}{c})} e^{j(\varphi_a - \varphi_b)} \\ & \cdot \sum_{m=1}^M w_{T,m}^c e^{j2\pi d \frac{\sin \theta}{c} [(m-1)f_c + (m-1)^2 \Delta f]}. \end{aligned} \quad (14)$$

Accordingly, the received FDA radar signal can be finally represented respectively by

$$\begin{aligned} & e^{-j2\pi f_c(\frac{2r}{c} - \frac{2r_{b,\min}}{c})} e^{j(\varphi_a - \varphi_b)} \\ & \cdot \sum_{m=1}^M \left\{ w_{T,m}^c e^{j2\pi d \frac{\sin \theta}{c} [(m-1)f_c + (m-1)^2 \Delta f]} \right\} \\ & \cdot e^{j2\pi(m-1)\Delta f(t - \frac{2r}{c})} \end{aligned} \quad (15)$$

$, t \in \left[\frac{2r}{c}, \frac{2r}{c} + T_p\right].$

$$\begin{aligned} & e^{-j2\pi(m'-1)\Delta f(t - \frac{2r}{c})} e^{-j2\pi(m'-1)\Delta f(\frac{2r}{c} - \frac{2r_{b,\min}}{c})} \\ & \cdot e^{-j2\pi f_c(\frac{2r}{c} - \frac{2r_{b,\min}}{c})} e^{j(\varphi_a - \varphi_b)} \\ & \cdot \sum_{m=1}^M \left\{ w_{T,m}^c e^{j2\pi d \frac{\sin \theta}{c} [(m-1)f_c + (m-1)^2 \Delta f]} \right\} \\ & \cdot e^{j2\pi(m-1)\Delta f(t - \frac{2r}{c})} \end{aligned} \quad (16)$$

$, t \in \left[\frac{2r}{c}, \frac{2r}{c} + T_p\right], m' = 1, 2, \dots, M.$

Comparing (15) and (16), we can make the following conclusions:

- 1) The traditional receiver scheme via single-carrier mixing that is widely adopted for phased-array and MIMO radars cannot generate the desired range-related steering vector in the received FDA signal models. In addition, the extra

where $\Upsilon = \int_{\frac{2r}{c}}^{\frac{2r}{c}+T_p} \tilde{\mathbf{y}}^c(t) [\mathbf{e}^T(t) e^{j2\pi f_c t}] s(t) dt$ is just the sufficient statistic for FDA radar. Note that the term $\mathbf{e}^T(t) e^{j2\pi f_c t}$ in Υ comes from the multi-carrier mixing operation. In doing so, the range-related terms are preserved in the FDA radar joint transmit-receive steering vector.

Fig. 2 illustrates the receiver structure, which is featured by the multiple mixers with frequencies f_1, f_2, \dots, f_M , essentially different from that for conventional MIMO and phased-array radars. The local mixing signal is

$$\text{rect}_g\left(\frac{t - 2r_{g,\min}/c}{T_g}\right) [\mathbf{e}^T(t) e^{j2\pi f_c t}]. \quad (24)$$

Then, after mixing it with (17), we can get

$$\begin{aligned} \mathbf{Z}(t) &= \mathbf{y}(t) \cdot \left(\text{rect}_g\left(\frac{t - 2r_{g,\min}/c}{T_g}\right) [\mathbf{e}^T(t) e^{j2\pi f_c t}] \right)^c \\ &= \varsigma(r, \theta) e^{j2\pi f_c (t - \frac{2r}{c})} s\left(t - \frac{2r}{c}\right) \\ &\quad \cdot \mathbf{a}_{R,\theta}(\theta) [\mathbf{w}^H \odot \mathbf{a}_{T,\theta}^T(\Delta f, \theta)] \\ &\quad \cdot \text{rect}\left(\frac{t - \frac{2r}{c}}{T_p}\right) \mathbf{e}\left(t - \frac{2r}{c}\right) \\ &\quad \cdot \text{rect}_g\left(\frac{t - 2r_{g,\min}/c}{T_g}\right) \mathbf{e}^H(t) e^{-j2\pi f_c t} \end{aligned} \quad (25)$$

Moreover, we have

$$\begin{aligned} &e^{j2\pi f_c (t - \frac{2r}{c})} \text{rect}\left(\frac{t - \frac{2r}{c}}{T_p}\right) \mathbf{e}\left(t - \frac{2r}{c}\right) \\ &\quad \cdot \text{rect}_g\left(\frac{t - 2r_{g,\min}/c}{T_g}\right) \mathbf{e}^H(t) e^{-j2\pi f_c t} \\ &= e^{j(\phi_a - \phi_b)} e^{j2\pi f_c \left(\frac{2r_{b,\min}}{c} - \frac{2r}{c}\right)} \\ &\quad \cdot \text{rect}\left(\frac{t - \frac{2r}{c}}{T_p}\right) \text{rect}_g\left(\frac{t - 2r_{g,\min}/c}{T_g}\right) \\ &\quad \cdot \mathbf{e}\left(t - \frac{2r}{c}\right) \mathbf{e}^H\left(t - \frac{2r}{c}\right) \text{diag}\left\{\mathbf{e}\left(\frac{2r_{b,\min}}{c} - \frac{2r}{c}\right)\right\} \end{aligned} \quad (26)$$

Substituting (26) into (25) yields

$$\begin{aligned} \mathbf{Z}(t) &= \vartheta(r, \theta) \text{rect}_g\left(\frac{t - 2r_{g,\min}/c}{T_g}\right) \\ &\quad \cdot \mathbf{a}_{R,\theta}(\theta) [\mathbf{w}^H \odot \mathbf{a}_{T,\theta}^T(\Delta f, \theta)] \\ &\quad \cdot \text{rect}\left(\frac{t - 2r/c}{T_p}\right) s\left(t - \frac{2r}{c}\right) \\ &\quad \cdot \mathbf{e}\left(t - \frac{2r}{c}\right) \mathbf{e}^H\left(t - \frac{2r}{c}\right) \text{diag}\{\beta_{R,r}(\Delta f, r)\} \end{aligned} \quad (27)$$

where $\vartheta(r, \theta) = \varsigma(r, \theta) e^{j(\phi_a - \phi_b)} e^{j2\pi f_c \left(\frac{2r_{b,\min}}{c} - \frac{2r}{c}\right)}$, and the receiving range-related steering vector is

$$\begin{aligned} \beta_{R,r}(\Delta f, r) &= \mathbf{e}\left(\frac{2r_{b,\min}}{c} - \frac{2r}{c}\right) \\ &= \begin{bmatrix} 1 & e^{-j2\pi \Delta f \frac{(r_{b,\min} - r)}{c}} & \dots & e^{-j2\pi(M-1)\Delta f \frac{(r_{b,\min} - r)}{c}} \end{bmatrix}^T \end{aligned} \quad (28)$$

Considering the FDA sufficient statistics Υ , the next step is to matched filtering the mixed signal with the reference function:

$$\tilde{s}(t) = \text{rect}\left(\frac{t - 2r_{g,\min}/c}{T_p}\right) s^c\left(T_p - t + \frac{2r_{g,\min}}{c}\right) \quad (29)$$

In doing so, the received FDA signal can be finally expressed as

$$\begin{aligned} \hat{\mathbf{R}}_{FDA}(t) &= \mathbf{Z}(t) * \tilde{s}(t) \\ &= \vartheta(r, \theta) \mathbf{a}_{R,\theta}(\theta) [\mathbf{w}^H \odot \mathbf{a}_{T,\theta}^T(\Delta f, \theta)] \\ &\quad \cdot \mathbf{V}(t) \text{diag}\{\beta_{R,r}(\Delta f, r)\} \\ &\quad , t \in \left[\frac{4r_{g,\min}}{c}, \frac{2r_{g,\min}}{c} + \frac{2r_{g,\max}}{c} + T_p\right] \end{aligned} \quad (30)$$

where $\mathbf{V}(t)$ is

$$\begin{aligned} \mathbf{V}(t) &= \begin{bmatrix} \text{rect}\left(\frac{t - 2r/c}{T_p}\right) s\left(t - \frac{2r}{c}\right) \\ \cdot \mathbf{e}\left(t - \frac{2r}{c}\right) \mathbf{e}^H\left(t - \frac{2r}{c}\right) \end{bmatrix} \\ &\quad * \left[\text{rect}\left(\frac{t - 2r_{g,\min}/c}{T_p}\right) s^c\left(T_p - t + \frac{2r_{g,\min}}{c}\right) \right] \end{aligned} \quad (31)$$

For comparison, we also write out the corresponding results for an $M \times N$ phased-array radar as [24]

$$\begin{aligned} \mathbf{r}_{PA}(t) &= \vartheta(r, \theta) u(t) \mathbf{a}_{R,\theta}(\theta) \mathbf{w}^H \mathbf{a}_{T,\theta}(\Delta f, \theta) \\ &\quad , t \in \left[\frac{4r_{g,\min}}{c}, \frac{2r_{g,\min}}{c} + \frac{2r_{g,\max}}{c} + T_p\right] \end{aligned} \quad (32)$$

Accordingly, $u(t)$ is expressed as

$$\begin{aligned} u(t) &= \left[\text{rect}\left(\frac{t - 2r/c}{T_p}\right) s\left(t - \frac{2r}{c}\right) \right] \\ &\quad * \left[\text{rect}\left(\frac{t - 2r_{g,\min}/c}{T_p}\right) s^c\left(T_p - t + \frac{2r_{g,\min}}{c}\right) \right]. \end{aligned} \quad (33)$$

It is noticed that (31) exhibits significant difference from (33):

- 1) $\mathbf{r}_{PA}(t)$ has amplitude peak at $t = \frac{4r_{g,\min}}{c} + \frac{2r_{g,\max}}{c} + T_p$, which implies that phased-array radar can estimate directly target range from the peak position. However, for FDA, each column of $\mathbf{V}(t)$ may not have an amplitude peak at $t = \frac{4r_{g,\min}}{c} + \frac{2r_{g,\max}}{c} + T_p$.
- 2) For phased-array radar, the sampling output at the peak of $\mathbf{r}_{PA}(t)$ has maximum signal-to-noise ratio (SNR), but the FDA matrix $\mathbf{V}(t)$ may have multiple peaks if a large FO is adopted, which will reduce the output energy in each channel. Nevertheless, the output SNR can be enhanced by utilizing the frequency diversity of FDA.
- 3) The range-related matrix $\text{diag}[\beta_{R,r}(\Delta f, r)]$ in $\hat{\mathbf{R}}_{FDA}(t)$ enables FDA to estimate target range through, for example, subspace algorithms [25], and even for super-resolution ranging.

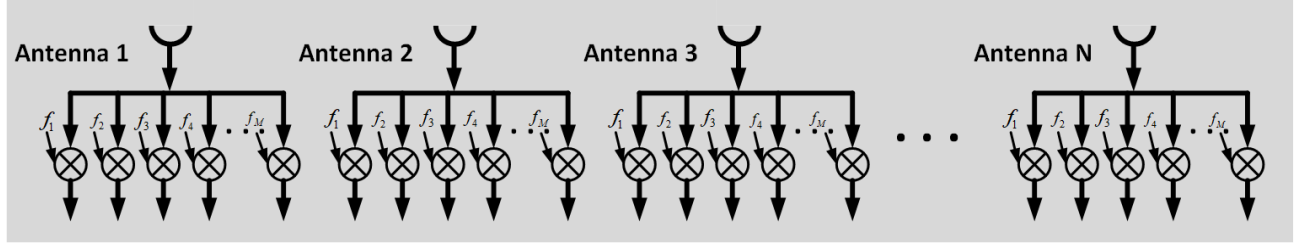


Fig. 2. FDA multi-carrier mixing receiver structure.

III. JOINT TRANSMIT-RECEIVE ARRAY WEIGHTERS OPTIMIZATION

In this Section, we jointly optimize the transmit and receive weighting vectors for coherent FDA radar systems. Our purpose is to maximize the energy radiated within the desired range-angle section to the total radiated energy.

A. Optimization Problem Formulation

Since the derived FDA beampattern in (6) is time-dependent, we can integrate it over the pulse duration to eliminate the influence of time on the beampattern. Then, we can define the FDA integral transmit beampattern (FGTB) as

$$P_{\text{FGTB}}(\mathbf{w}, \Delta f, \theta) = \int_{r/c}^{r/c+T_p} r_T(t) r_T^c(t) dt$$

$$= \int_0^{T_p} \left\{ s(t) s^c(t) \mathbf{w}^H [\mathbf{e}(t) \odot \mathbf{a}_{T,\theta}(\Delta f, \theta)] \right\} dt \quad (34)$$

$$= \text{Tr} \left\{ \mathbf{R}_{\text{FDA}} [\mathbf{w}^c \odot \alpha_{\text{FDA}, \Delta f}(\theta)]^c \right\}$$

where $\mathbf{R}_{\text{FDA}} = \int_0^{T_p} s(t) \mathbf{e}(t) \mathbf{e}^H(t) s^c(t) dt \in \mathbb{C}^{M \times M}$ is the correlation matrix of the FDA transmitted signals. Then, we make the following conclusions [12]:

- 1) For $(M-1)\Delta f \ll B_{s(t)}$, we have $\mathbf{R}_{\text{FDA}} \approx \mathbf{I}_M$. In this case, the transmit waveforms remain good coherence, just like the phased-array, we refer to it as coherent FDA. Its FGTB can be approximately written as

$$P_{\text{C-FDA}}(\mathbf{w}, \Delta f, \theta) \approx \mathbf{w}^H \mathbf{a}_{T,\theta}(\Delta f, \theta) \mathbf{a}_{T,\theta}^H(\Delta f, \theta) \mathbf{w}$$

$$= \mathbf{w}^H \mathbf{T}(\Delta f, \theta) \mathbf{w} \quad (35)$$

where $\mathbf{T}(\Delta f, \theta) = \mathbf{a}_{T,\theta}(\Delta f, \theta) \mathbf{a}_{T,\theta}^H(\Delta f, \theta)$ and subscript C-FDA means coherent FDA radar.

- 2) For $\Delta f > B_{s(t)}$, we have $\mathbf{R}_{\text{FDA}} \approx \mathbf{I}_M$. The corresponding FGTB will be

$$P_{\text{FDA-MIMO}}(\mathbf{w}, \Delta f, \theta) \approx \mathbf{w}^H \mathbf{w} \quad (36)$$

This case is actually equivalent to the FDA-MIMO model [26], which is non-coherent without directional array gain.

For FDA transmitter, we hope to focus the transmit energy to the interested spatial sections. Therefore, the transmit

weighting vector \mathbf{w} should maximize the integrated mainlobe-to-sidelobe ratio of the coherent FDA FGTB. That is

$$P_1 : \begin{cases} \max_{\mathbf{w}} & \frac{\oint_{D_t} [\mathbf{w}^H \mathbf{T}(\Delta f, \theta) \mathbf{w}] d\theta}{\oint_{D_s} [\mathbf{w}^H \mathbf{T}(\Delta f, \theta) \mathbf{w}] d\theta} = \frac{\mathbf{w}^H \mathbf{\Omega}_t \mathbf{w}}{\mathbf{w}^H \mathbf{\Omega}_s \mathbf{w}} \\ \text{s. t.} & (M-1)\Delta f \ll B_{s(t)} \end{cases} \quad (37)$$

where D_t and D_s represent the potential spatial sections of interest and sidelobe regions, respectively. $\mathbf{\Omega}_t = \oint_{D_t} \mathbf{T}(\Delta f, \theta) d\theta$ and $\mathbf{\Omega}_s = \oint_{D_s} \mathbf{T}(\Delta f, \theta) d\theta$.

The optimal solution $\hat{\mathbf{w}}$ to the problem P_1 is $\hat{\mathbf{w}} = \lambda_{\max, \text{vec}} \{ \mathbf{\Omega}_s^{-1} \mathbf{\Omega}_t \}$.

Proof: See Appendix A.

Although the transmit weighting vector $\hat{\mathbf{w}}$ enables the transmit energy to concentrate within the interested spatial sectors as much as possible, it does not guarantee the maximum receive energy in the desired two-dimensional range-angle sections. To this end, in the following, we propose a joint scheme to optimize the transmit and receive weighting vectors.

For a coherent FDA radar, i.e., $(M-1)\Delta f \ll B_{s(t)}$, we have $\mathbf{V}(t) \approx \mathbf{I}_M$. Then, according to (33), the received signal $\hat{\mathbf{R}}_{\text{C-FDA}} \in \mathbb{C}^{N \times M}$ should be

$$\hat{\mathbf{R}}_{\text{C-FDA}} = \vartheta(r, \theta) \mathbf{a}_{R,\theta}(\theta) \mathbf{w}^H \mathbf{Q}(\Delta f, \theta, r) \quad (38)$$

with $\mathbf{Q}(\Delta f, \theta, r) = \mathbf{a}_{T,\theta}(\Delta f, \theta) \beta_{R,r}(\Delta f, r)$. Stacking (41) in a tall vector, we get the coherent FDA radar data vector $\mathbf{y}_{\text{C-FDA}} \in \mathbb{C}^{NM}$:

$$\mathbf{y}_{\text{C-FDA}} = \text{vec} \{ \hat{\mathbf{R}}_{\text{C-FDA}} \} = \mathbf{w}^H \mathbf{T}(\Delta f, \theta) \mathbf{w}$$

$$= \vartheta(r, \theta) \text{vec} \{ \mathbf{a}_{R,\theta}(\theta) \mathbf{w}^H \mathbf{Q}(\Delta f, \theta, r) \} \quad (39)$$

$$= \vartheta(r, \theta) [\mathbf{Q}^T(\Delta f, \theta, r) \otimes \mathbf{a}_{R,\theta}(\theta)] \mathbf{w}^c$$

The equivalent receive beampattern can then be expressed as

$$\tilde{\Delta}(\mathbf{w}, \mathbf{b}) = |\mathbf{b}^H \mathbf{y}_{\text{C-FDA}}|^2 \quad (40)$$

where $\mathbf{b} \in \mathbb{C}^{NM}$ is just the receive weighting vector.

Finally, the objective function of the joint transmit and receive weighting vectors optimization problem for coherent FDA can be formulated as

$$\Delta(\mathbf{w}, \mathbf{b}) = \frac{\oint_{\Theta_t} \tilde{\Delta}(\mathbf{w}, \mathbf{b}) d\theta dr}{\oint_{\Theta} \tilde{\Delta}(\mathbf{w}, \mathbf{b}) d\theta dr} \quad (41)$$

$$\Theta : \begin{cases} -\frac{\pi}{2} \leq \theta \leq \frac{\pi}{2} \\ r_{g,\min} \leq r \leq r_{g,\max} \end{cases}$$

where Θ_t and Θ denote the interested two-dimensional range-angle sections and the whole potential sections, respectively.

B. Constrains

Our purpose is to design the transmit weight vector \mathbf{w} and the receive weight vector \mathbf{b} by maximizing the ratio of the energy radiated within the desired range-angle two-dimensional spatial section to the total radiated energy. However, in practical applications, additional constraints must be considered.

First is similarity constraint. Similarity constraint has been widely used in MIMO radar waveform design [27]–[29]. For FDA, enforcing a similarity constraint on the transmit weight vector allows a compromise between optimizing the output power and controlling the transmit beampattern. This is equivalent to optimizing the output power in a suitable neighborhood of a reference transmit weight vector which is known to have good properties.

We assume that $\mathbf{w}_0 = \hat{\mathbf{w}}$ is the reference transmit weight vector, and consider the following similarity constraint:

$$\|\mathbf{w} - \rho \mathbf{w}_0\| \leq 1, \quad |\rho|^2 \leq 1 \quad (42)$$

where ρ is a real parameter controlling the level of the similarity.

The second is the constraint on the transmit energy of each coherent FDA array element. Due to the limit of nonlinear radar amplifiers, it is expected that the transmit energy of each array element should be no larger than a threshold [23], [30].

And for coherent-FDA, from (1), the energy radiated by the m th array element can be expressed as

$$\begin{aligned} & \int_{T_p} \left| w_{t,m}^c s(t) e^{j2\pi(m-1)\Delta f t} \right|^2 dt \\ &= \int_{T_p} |w_{t,m}^c|^2 |s(t)|^2 dt = |w_{t,m}^c|^2 \int_{T_p} |s(t)|^2 dt \\ &= |w_{t,m}^c|^2, \quad m = 1, 2, \dots, M \end{aligned} \quad (43)$$

Therefore, the energy constraint for coherent FDA can be written as

$$\mathbf{w}^H \mathbf{E}_m \mathbf{w} \leq \frac{1}{M}, \quad m = 1, \dots, M-1 \quad (44)$$

$$\text{where } \mathbf{E}_m(i, j) = \begin{cases} 1, & i = m \text{ and } j = m \\ 0, & \text{otherwise} \end{cases}.$$

C. Optimization Algorithm Implementation

According to the above discussions, the problem of coherent FDA joint design of the transmit weight and receive weight vectors subject to the aforementioned constraints can be formulated as

$$\begin{aligned} & \max_{\mathbf{w}, \mathbf{b}} \quad \Delta(\mathbf{w}, \mathbf{b}) \\ & \text{s. t.} \quad \begin{cases} \|\mathbf{w} - \rho \mathbf{w}_0\| \leq 1, |\rho|^2 \leq 1 \\ \mathbf{w}^H \mathbf{E}_m \mathbf{w} \leq \frac{1}{\sqrt{M}}, m = 1, \dots, M-1 \end{cases} \end{aligned} \quad (45)$$

In order to obtain the integration value of the objective function $\Delta(\mathbf{w}, \mathbf{b})$, we adopt a sufficient approximation technique

by choosing dense grid points in the whole observation region. And, the optimization problem can then be written as

$$P_2 \begin{cases} \max_{\mathbf{w}, \mathbf{b}} & \frac{\sum_{(t_1, t_2)=(1,1)}^{(T_1, T_2)} |\mathbf{b}^H \mathbf{G}(\Delta f, \theta_{t_1}, r_{t_2}) \mathbf{w}^c|^2}{\sum_{g=1}^{J_1} \sum_{h=1}^{J_2} |\mathbf{b}^H \mathbf{G}(\Delta f, \theta_g, r_h) \mathbf{w}^c|^2} \\ \text{s. t.} & \begin{cases} \|\mathbf{w} - \rho \mathbf{w}_0\| \leq 1, |\rho|^2 \leq 1 \\ \mathbf{w}^H \mathbf{E}_m \mathbf{w} \leq \frac{1}{M}, m = 1, \dots, M \end{cases} \end{cases} \quad (46)$$

where T_1 and T_2 denote the number of grid points in the angle dimension and range dimension in the desired area, respectively. And J_1 and J_2 denote the number of grid points in the angle dimension and range dimension in the whole observation region, respectively.

Then, following the results in [31], the problem P_2 can be converted to

$$P_3 \begin{cases} \max_{\mathbf{w}, \mathbf{b}} & \frac{\sum_{(t_1, t_2)=(1,1)}^{(T_1, T_2)} |\mathbf{b}^H \mathbf{G}(\Delta f, \theta_{t_1}, r_{t_2}) \mathbf{w}^c|^2}{\sum_{g=1}^{J_1} \sum_{h=1}^{J_2} |\mathbf{b}^H \mathbf{G}(\Delta f, \theta_g, r_h) \mathbf{w}^c|^2} \\ \text{s. t.} & \begin{cases} \mathbf{w}^H \mathbf{\Gamma}(\mathbf{w}_0) \mathbf{w} \leq 1 \\ \mathbf{w}^H \mathbf{E}_m \mathbf{w} \leq \frac{1}{M}, m = 1, \dots, M \end{cases} \end{cases} \quad (47)$$

where $\mathbf{\Gamma}(\mathbf{w}_0) = \mathbf{I}_M - \mathbf{w}_0 \mathbf{w}_0^H$.

Since the objective function is a quadratic fractional function with respect to \mathbf{w} and \mathbf{b} , problem P_3 is nonconvex and NP-hard problem [32]. Therefore, there has no effective method to solve this problem. In the following, an iterative method is devised, eventually yielding the optimal parameters $(\mathbf{w}^*, \mathbf{b}^*)$.

We first summarize the steps of the proposed algorithm and then describe each step in detail.

- 1) Optimize the receive weight vector \mathbf{b} for a given transmit weight vector \mathbf{w} based on the results in the Appendix.
- 2) Optimize the transmit weight vector \mathbf{w} for a given receive weight vector \mathbf{b} based on the semidefinite relaxation (SDR) and randomization techniques.
- 3) Iterate Steps 1 and 2 until a practical convergence criterion is satisfied.

1) *Optimization of \mathbf{b} :* For a given \mathbf{w} , the problem P_3 can be expressed as

$$\max_{\mathbf{b}} \frac{\sum_{(t_1, t_2)=(1,1)}^{(T_1, T_2)} |\mathbf{b}^H \mathbf{G}(\Delta f, \theta_{t_1}, r_{t_2}) \mathbf{w}^c|^2}{\sum_{g=1}^{J_1} \sum_{h=1}^{J_2} |\mathbf{b}^H \mathbf{G}(\Delta f, \theta_g, r_h) \mathbf{w}^c|^2}. \quad (48)$$

And it can then be simplified to the following problem

$$P_4 \left\{ \max_{\mathbf{b}} \frac{\mathbf{b}^H \tilde{\Pi}(\mathbf{w}) \mathbf{b}}{\mathbf{b}^H \Pi(\mathbf{w}) \mathbf{b}} \right. \quad (49)$$

where

$$\Pi(\mathbf{w}) = \sum_{g=1}^{J_1} \sum_{h=1}^{J_2} \mathbf{G}(\Delta f, \theta_g, r_h) \mathbf{w} \mathbf{w}^H \mathbf{G}^H(\Delta f, \theta_g, r_h) \quad (50)$$

and

$$\tilde{\Pi}(\mathbf{w}) = \sum_{(t_1, t_2)=(1,1)}^{(T_1, T_2)} \mathbf{G}(\Delta f, \theta_{t_1}, r_{t_2}) \mathbf{w} \mathbf{w}^H \mathbf{G}^H(\Delta f, \theta_{t_1}, r_{t_2}). \quad (51)$$

Note that problem P_4 is similar to problem P_1 . Therefore, we can get the analytical solution of the P_4 as follows

$$\mathbf{b}^* = \lambda_{\max, vec} \left\{ \Pi(\mathbf{w})^{-1} \tilde{\Pi}(\mathbf{w}) \right\}. \quad (52)$$

2) *Optimization of \mathbf{w}* : For the objective function in problem P_3 , maximizing the ratio is equivalent to maximizing the numerator while fixing the denominator. As a result, problem P_3 can be rewritten as

$$\begin{aligned} \max_{\mathbf{w}} \quad & \sum_{g=1}^{J_1} \sum_{h=1}^{J_2} |\mathbf{b}^H \mathbf{G}(\Delta f, \theta_g, r_h) \mathbf{w}^c|^2 \\ \text{s. t.} \quad & \begin{cases} \mathbf{w}^H \mathbf{\Gamma}(\mathbf{w}_0) \mathbf{w} \leq 1 \\ \mathbf{w}^H \mathbf{E}_m \mathbf{w} \leq \frac{1}{M}, m = 1, \dots, M \\ \sum_{(t_1, t_2) \in (1, 1)}^{(T_1, T_2)} |\mathbf{b}^H \mathbf{G}(\Delta f, \theta_{t_1}, r_{t_2}) \mathbf{w}^c|^2 = 1 \end{cases} \end{aligned} \quad (53)$$

And it can then be simplified to the following problem

$$P_5 \begin{cases} \min_{\mathbf{w}} & \mathbf{w}^H \Xi(\mathbf{b}) \mathbf{w} \\ \text{s. t.} & \begin{cases} \mathbf{w}^H \mathbf{\Gamma}(\mathbf{w}_0) \mathbf{w} \leq 1 \\ \mathbf{w}^H \mathbf{E}_m \mathbf{w} \leq \frac{1}{M}, m = 1, \dots, M - 1 \\ \mathbf{w}^H \tilde{\Xi}(\mathbf{b}) \mathbf{w} = 1 \end{cases} \end{cases} \quad (54)$$

where

$$\Xi(\mathbf{b}) = \sum_{g=1}^{J_1} \sum_{h=1}^{J_2} \gamma(\mathbf{b}; \theta_{t_1}, r_{t_2}) \gamma^H(\mathbf{b}; \theta_{t_1}, r_{t_2}) \quad (55)$$

and

$$\tilde{\Xi}(\mathbf{b}) = \sum_{(t_1, t_2) \in (1, 1)}^{(T_1, T_2)} \gamma(\mathbf{b}; \theta_{t_1}, r_{t_2}) \gamma^H(\mathbf{b}; \theta_{t_1}, r_{t_2}) \quad (56)$$

with $\gamma(\mathbf{b}; \theta, r) = \mathbf{G}^H(\Delta f, \theta, r) \mathbf{b}$.

Note that the above optimization problem involves a non-convex quadratic equality constraint, and hence, it is a non-convex quadratically constrained quadratic program (QCQP) and there is no closed-form solution to the problem P_5 .

By introducing a new variable $\mathbf{W} = \mathbf{w} \mathbf{w}^H$ and noting that $\mathbf{W} = \mathbf{w} \mathbf{w}^H$ is equivalent to \mathbf{W} being a rank one symmetric positive semidefinite (PSD) matrix, we obtain the following equivalent formulation of P_5 :

$$P_6 \begin{cases} \min_{\mathbf{W}} & \text{Tr}(\Xi(\mathbf{b}) \mathbf{W}) \\ \text{s. t.} & \begin{cases} \text{Tr}(\mathbf{\Gamma}(\mathbf{w}_0) \mathbf{W}) \leq 1 \\ \text{Tr}(\mathbf{E}_m \mathbf{W}) \leq \frac{1}{M}, m = 1, \dots, M - 1 \\ \text{Tr}(\tilde{\Xi}(\mathbf{b}) \mathbf{W}) = 1 \\ \mathbf{W} \succeq \mathbf{0} \\ \mathbf{W} = \mathbf{w} \mathbf{w}^H \text{ or Rank}\{\mathbf{W}\} = 1 \end{cases} \end{cases} \quad (57)$$

It can be seen that problem P_6 can be easily solved by SDR technique. In particular, SDR is a powerful, computationally efficient technique and is capable of providing accurate approximation for the nonconvex QCQPs in an almost mechanical fashion [33].

First, we drop the nonconvex rank constraint $\text{Rank}\{\mathbf{W}\} = 1$ to obtain the following relaxed version of P_6 :

$$P_7 \begin{cases} \min_{\mathbf{W}} & \text{Tr}(\Xi(\mathbf{b}) \mathbf{W}) \\ \text{s. t.} & \begin{cases} \text{Tr}(\mathbf{\Gamma}(\mathbf{w}_0) \mathbf{W}) \leq 1 \\ \text{Tr}(\mathbf{E}_m \mathbf{W}) \leq \frac{1}{M}, m = 1, \dots, M - 1 \\ \text{Tr}(\tilde{\Xi}(\mathbf{b}) \mathbf{W}) = 1 \\ \mathbf{W} \succeq \mathbf{0} \end{cases} \end{cases} \quad (58)$$

Problem P_7 is a convex semidefinite programming (SDP) problem. And using the convex optimization toolbox CVX [34], we can solve it in MATLAB.

Now, if the SDP returns a solution whose rank satisfies the rank constraint, then that solution will be optimal for the problem P_6 . However, in most cases, the SDP solution is infeasible.

Next, we need to try to extract an approximate nonconvex QCQP solution from the SDR solutions. And randomization has been empirically found to provide promising approximations provided that a solution for sufficient number of randomization trials is employed [35]. Hence, a randomization method are adopt to obtain an approximate solution \mathbf{w}^* from the SDP solutions.

- 1) Suppose the solution of the SDP is \mathbf{W}^* . Then, the Cholesky factorization can be expressed as

$$\mathbf{W}^* = \mathbf{R}_w^H \mathbf{R}_w \quad (59)$$

where \mathbf{R}_w is an upper triangular matrix.

- 2) Generate independent identically distributed standard Gaussian $\sigma_k \sim N(0, \mathbf{I})$ random vectors $\sigma_k, k = 1, 2, \dots, K$ with K being the number of the randomization trials.
- 3) Construct new random vectors $\xi_k = \mathbf{R}_w^H \sigma_k, k = 1, 2, \dots, K$. Therefore, the covariance matrix of ξ_k is \mathbf{W}^* .

Note that the random samples ξ_k are not always feasible for the problem P_6 , but we can apply the following method to turn them into the feasible set.

First, apply a rescaling method yields new random vectors

$$\varsigma_k = \frac{\xi_k}{\sqrt{\xi_k^H \gamma(\mathbf{b}; \theta, r) \gamma^H(\mathbf{b}; \theta, r) \xi_k}}, \quad k = 1, 2, \dots, K \quad (60)$$

Note that the new random vectors ς_k satisfy the equality constraint $\text{Tr}(\tilde{\Xi}(\mathbf{b}) \varsigma_k \varsigma_k^H) = 1$. And we can also obtain the following equations:

$$\begin{aligned} \varsigma_k^H \mathbf{\Gamma}(\mathbf{w}_0) \varsigma_k &= \xi_k^H \mathbf{\Gamma}(\mathbf{w}_0) \xi_k \\ \varsigma_k^H \mathbf{E}_m \varsigma_k &= \xi_k^H \mathbf{E}_m \xi_k, \quad m = 1, \dots, M - 1 \end{aligned} \quad (61)$$

Then, select the desired random variables $\vartheta_l, l = 1, 2, \dots, L$ from the set $R_1(\varsigma_k) \cap R_2(\varsigma_k)$ with $R_1(\varsigma_k)$ being defined as

$$R_1(\varsigma_k) = \{\varsigma_k \mid \varsigma_k^H \mathbf{\Gamma}(\mathbf{w}_0) \varsigma_k \leq 1\} \quad (62)$$

and $R_2(\varsigma_k)$ is given by

$$R_2(\varsigma_k) = \left\{ \varsigma_k \mid \varsigma_k^H \mathbf{E}_m \varsigma_k \leq \frac{1}{M} \right\}, \quad m = 1, \dots, M - 1 \quad (63)$$

Finally, the optimal transmit weight vector $\mathbf{w}^* = \vartheta^*$ is obtained with

$$\vartheta^* = \arg \min_{\vartheta_l} \vartheta_l^H \Xi(\mathbf{b}) \vartheta_l, \quad l = 1, 2, \dots, L \quad (64)$$

According to the above analysis, the proposed iterative algorithm is summarized as follows.

Algorithm 1 The Proposed Iterative Algorithm:

Input: T target locations

$(\theta_{t,1}, r_{t,1}), (\theta_{t,2}, r_{t,2}), \dots, (\theta_{t,T}, r_{t,T})$, potential spatial sections D_t and sidelobe regions D_s .

Output: The optimal transmit and receive weight vectors $(\mathbf{w}^*, \mathbf{b}^*)$.

1: Compute

$$\Omega_t = \oint_{D_t} \mathbf{T}(\Delta f, \theta) d\theta,$$

$$\Omega_s = \oint_{D_s} \mathbf{T}(\Delta f, \theta) d\theta,$$

$$\mathbf{T}(\Delta f, \theta) = \mathbf{a}_{T,\theta}(\Delta f, \theta) \mathbf{a}_{T,\theta}^H(\Delta f, \theta).$$

Obtain the reference transmit weight vector $\mathbf{w}_0 = \lambda_{\max, \text{vec}} \{ \Omega_s^{-1} \Omega_t \}$.

2: For $q = 1$, initialize the transmit weight vector $\mathbf{w}_1 = \mathbf{w}_0$.

3: Let $q = q + 1$, compute

$$\Pi(\mathbf{w}_{q-1}) = \sum_{g=1}^{J_1} \sum_{h=1}^{J_2} \left\{ \mathbf{G}(\Delta f, \theta_g, r_h) \mathbf{w}_{q-1} \right. \\ \left. \times \mathbf{w}_{q-1}^H \mathbf{G}^H(\Delta f, \theta_g, r_h) \right\},$$

$$\tilde{\Pi}(\mathbf{w}_{q-1}) = \sum_{i=1}^T \left\{ \mathbf{G}(\Delta f, \theta_i, r_i) \mathbf{w}_{q-1} \right. \\ \left. \times \mathbf{w}_{q-1}^H \mathbf{G}^H(\Delta f, \theta_i, r_i) \right\},$$

$$\mathbf{G}(\Delta f, \theta, r) = \mathbf{a}_{T,\theta}(\Delta f, \theta) \beta_{R,r}(\Delta f, r).$$

Obtain

$$\mathbf{b}_{q-1} = \lambda_{\max, \text{vec}} \{ \Pi(\mathbf{w}_{q-1})^{-1} \tilde{\Pi}(\mathbf{w}_{q-1}) \}.$$

4: Compute

$$\Xi(\mathbf{b}_{q-1}) = \sum_{g=1}^{J_1} \sum_{h=1}^{J_2} \gamma(\mathbf{b}_{q-1}; \theta_{t_1}, r_{t_2}) \gamma^H(\mathbf{b}_{q-1}; \theta_{t_1}, r_{t_2}),$$

$$\tilde{\Xi}(\mathbf{b}_{q-1}) = \sum_{i=1}^T \gamma(\mathbf{b}_{q-1}; \theta_{t,i}, r_{t,i}) \gamma^H(\mathbf{b}_{q-1}; \theta_{t,i}, r_{t,i}),$$

$$\gamma(\mathbf{b}_{q-1}, \theta, r) = \mathbf{G}^H(\Delta f, \theta, r) \mathbf{b}_{q-1}.$$

Solve the SDP problem below and denote by $\hat{\mathbf{W}}$ a solution of

$$\begin{aligned} \min_{\mathbf{W}} \quad & \text{Tr}(\Xi(\mathbf{b}_{q-1}) \mathbf{W}) \\ \text{s. t.} \quad & \begin{cases} \text{Tr}(\Gamma(\mathbf{w}_0) \mathbf{W}) \leq 1 \\ \text{Tr}(\mathbf{E}_m \mathbf{W}) \leq \frac{1}{M}, m = 1, \dots, M-1 \\ \text{Tr}(\tilde{\Xi}(\mathbf{b}_{q-1}) \mathbf{W}) = 1 \\ \mathbf{W} \succeq \mathbf{0} \end{cases} \end{aligned} \quad (65)$$

5: Perform the eigenvalue decomposition of $\hat{\mathbf{W}}$, i.e. $\hat{\mathbf{W}} = \mathbf{V} \Delta \mathbf{V}^H$.

6: If $\text{Rank}\{\mathbf{V}\} = 1$, then $\mathbf{V} = \mathbf{v} \mathbf{v}^H$, output $\mathbf{w}_q = \mathbf{v}$ and skip to Step 8.

7: Run randomization method steps as follows:

- Perform the Cholesky factorization $\hat{\mathbf{W}} = \mathbf{R}_w^H \mathbf{R}_w$;
- Generate independent identically distributed standard Gaussian $\sigma_k \sim N(0, \mathbf{I})$ random vectors $\sigma_k, k = 1, 2, \dots, K$ with K being the number of the randomization trials;
- For the k th randomization trial, let

$$\xi_k = \mathbf{R}_w^H \sigma_k, k = 1, 2, \dots, K;$$

- Apply a rescaling method

$$\varsigma_k = \frac{\xi_k}{\sqrt{\xi_k^H \gamma(\mathbf{b}_{q-1}; \theta, r) \gamma^H(\mathbf{b}_{q-1}; \theta, r) \xi_k}}, \quad k = 1, 2, \dots, K;$$

- Select $\vartheta_l, l = 1, 2, \dots, L$ from set $R_1(\varsigma_k) \cap R_2(\varsigma_k)$;

$$R_1(\varsigma_k) = \{ \varsigma_k \mid \varsigma_k^H \Gamma(\mathbf{w}_0) \varsigma_k \leq \kappa^2 \}$$

$$R_2(\varsigma_k) = \{ \varsigma_k \mid \varsigma_k^H \mathbf{E}_m \varsigma_k \leq \frac{1}{M} \}, \quad m = 1, \dots, M-1$$

with L being the number of the feasible trials;

- Choose $\mathbf{w}_q = \vartheta^*$ such that

$$\vartheta^* = \arg \min_{\vartheta_l} \vartheta_l^H \Xi(\mathbf{b}_{q-1}) \vartheta_l, l = 1, 2, \dots, L;$$

8: Compute the output energy

$$E_q = \mathbf{b}_{q-1}^H \Pi(\mathbf{w}_q) \mathbf{b}_{q-1}.$$

- 9: If $|E_q - E_{q-1}| \leq \kappa$ where κ is a user-defined parameter to control the convergence. Output $\mathbf{w}^* = \mathbf{w}_q$ and $\mathbf{b}^* = \mathbf{b}_{q-1}$. Otherwise, repeat Step 3.
-

IV. SIMULATION

In this section, we provide various numerical simulations to verify the performance of the proposed multi-channel mixing receiver and designed joint transmit-receive optimization algorithm for coherent FDA systems.

To this end, a narrowband coherent FDA radar system in which standard uniform FDA arrays with $M = 10$, $N = 10$ antennas are deployed in transmit and receive ends, respectively. Besides, the array parameters are set as interelement spacing $d = \frac{c}{2[f_c + (M-1)\Delta f]}$, the carrier frequency $f_c = 10 \text{ GHz}$ and FO $\Delta f = 5 \text{ kHz}$. Additionally, the transmitted baseband complex waveform $s(t)$ is linear frequency modulation signal, with bandwidth of $B_{s(t)} = 70 \text{ MHz}$, pulse duration $T_p = 10 \mu\text{s}$ and pulse repetition time $T_{\text{PRT}} = 300 \mu\text{s}$.

It should be noted that the coherent FDA receiver adopts the multi-carrier mixing structure shown in Fig. 2. And the radar range sampling gate $r_{g \max} - r_{g \min} = 25 \text{ km}$, the minimum radar range of interest $r_{g \min} = 60 \text{ km}$ and the maximum radar range of interest $r_{g \max} = 85 \text{ km}$ are considered in all subsequent simulations. That is, the total spatial sections of interest is $\Theta : \begin{cases} -90^\circ \leq \theta \leq 90^\circ \\ 60 \text{ km} \leq r \leq 85 \text{ km} \end{cases}$. Furthermore, for the proposed joint design algorithm, the number of randomization trials $Q = 200$.

1) *Example 1: Single Target:* In the simulation, the potential spatial sections of interest for the transmitter is $D_t : 40^\circ \leq \theta \leq 60^\circ$ and the target is located at $(50^\circ, 80 \text{ km})$ with a mesh grid size of $(0.2^\circ, 0.1 \text{ km})$.

The comparison between the transmit beampattern obtained with the reference transmit weight vector and the transmit beam pattern designed with the optimized transmit weight vector is shown in Fig. 3. The result in Fig. 3 reveals that the designed transmit beampattern has larger mainlobe width and higher sidelobe. This is not particularly surprising thing. In order to achieve optimal energy focusing at the coherent FDA receiver, the transmit weight vector and receive weight vector need to cooperate with each other, so the performance of the partially transmit beampattern is inevitably sacrificed. The performance loss of transmit beampattern will be more obvious in multi-target scenarios.

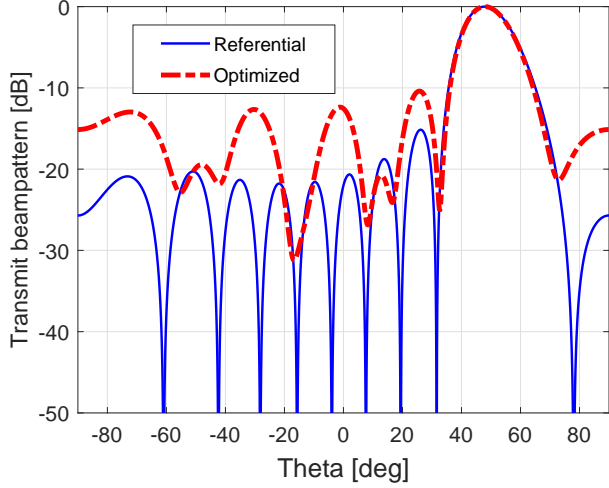


Fig. 3. Comparison between the optimized transmit beampattern and the reference transmit beampattern (single target).

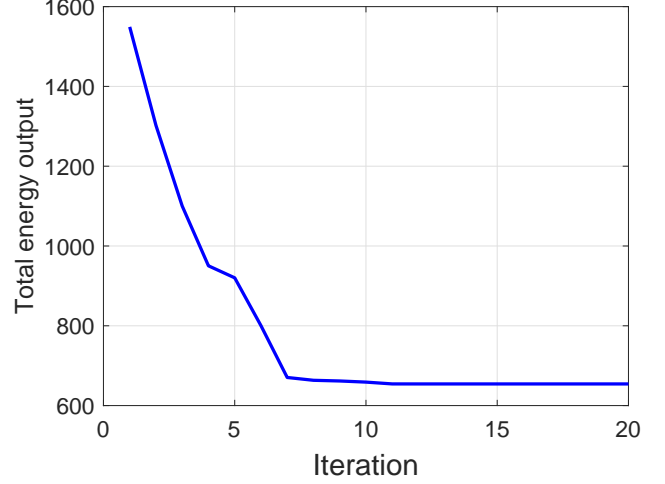


Fig. 5. The output energy of the whole region of interest versus the iteration number.

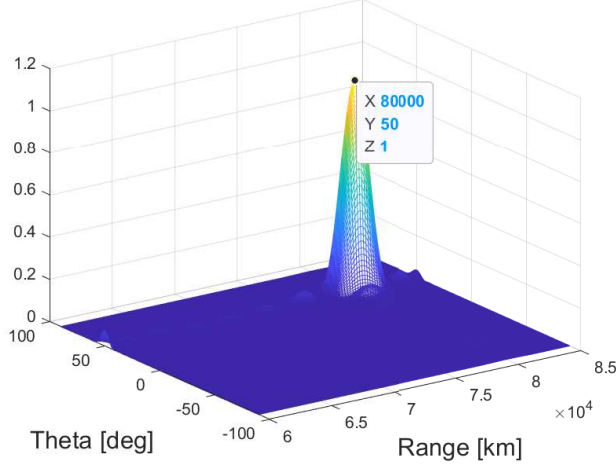


Fig. 4. Energy distribution of the coherent FDA radar echo in receiver end.

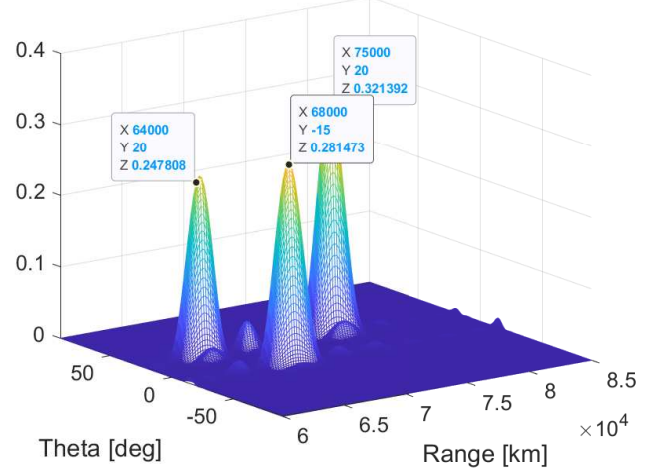


Fig. 6. 3-D transmit-receive beampattern.

In Fig. 4, we illustrate the energy distribution of the coherent FDA radar echo processed by the designed algorithm in the two-dimensional range-angle spatial sections. As expected, the designed multi-channel mixing receiver and joint transmit-receive optimization algorithm show excellent energy aggregation ability in both the range and the angle dimensions, with single energy peak and extremely low sidelobe.

The range-related steering vector provides coherent FDA with the potential of joint processing of radar echos in range and angle dimensions. However, phased-array and MIMO radars can only guide the energy of echo signals to the desired azimuth due to the lack of design DoF in range dimension.

Fig. 5 plots the achievable output energy of the entire detection region of interest $(\mathbf{b}^*)^H \Pi(\mathbf{w}^*) \mathbf{b}^*$ versus the iteration number during the execution of the designed optimization algorithm. Thanks to the excellent characteristics of SDR techniques, we can observe that the energy output converges very fast (after about 8-12 iterations).

2) *Example 2: Multiple Targets:* In the first example, we consider the case with three targets, two of which are located at the same angle. And the potential spatial sections of interest for transmitter is $D_t = [-40^\circ, -10^\circ] \cup [10^\circ, 30^\circ]$ with a mesh grid size of $(0.1^\circ, 0.1 \text{ km})$. The three targets are located at $(-15^\circ, 68 \text{ km})$, $(20^\circ, 64 \text{ km})$ and $(20^\circ, 75 \text{ km})$.

Fig. 6 shows the output energy distribution at the coherent FDA receiver. One can see that the echo energy is perfectly focused on the desired target position. In addition, in traditional phased-array and MIMO radars applications, since the angles of Target 2 and Target 3 are the same, these two targets exist in the mainlobe of the transmit beam, resulting in almost the same energy of the radar echo. This is a challenge to the traditional radar signal processing based on matched filtering and spatial beamforming.

Most importantly, for FDA, the joint processing ability of range and angle blurs the concept of mainlobe of the beam in traditional radar. Therefore, we can expect that for the

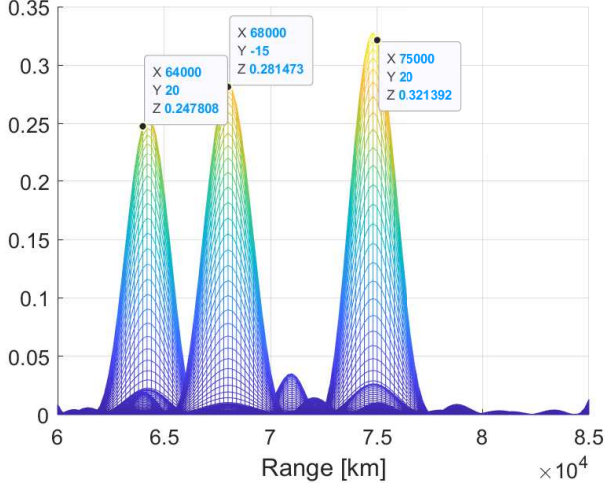


Fig. 7. Projection of the transmit-receive beampattern on range dimension.

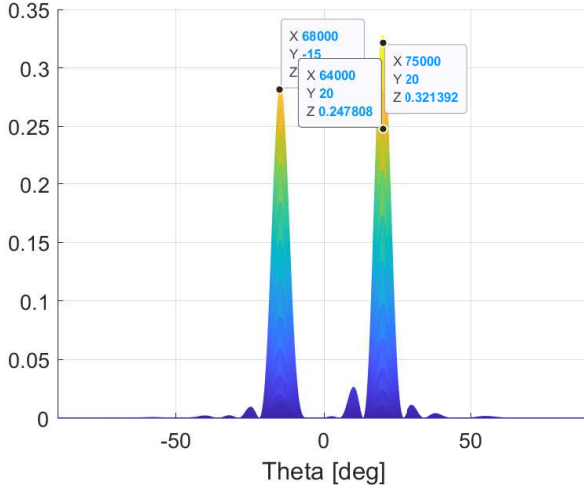


Fig. 8. Projection of the transmit-receive beampattern on angle dimension.

strong power interference located at the same azimuth of the target (the mainlobe interference), the coherent FDA can effectively suppress the energy of the interference and realize the detection to the desired target.

For clarity, Fig. 7 and Fig. 8 depict the obtained joint transmit-receive beampattern profiles in the range dimension and angle dimension, respectively. It is observed that the sidelobes are very low in both range and angle profiles. And it is worth noting that at the coherent FDA receiver end, although the total energy of the target area reaches the optimal, the energy allocation of each target cannot be well controlled. Controlling the output of each target will greatly increase the complexity of the algorithm, and the feasible set of the resultant optimization problem is likely to be an null set. That is, the obtained optimization problem is insoluble.

In the second example, we consider the case with three targets, two of which are located at the same range. And the potential spatial sections of interest for transmitter is $D_t = [-50^\circ, -10^\circ] \cup [10^\circ, 50^\circ]$ with a mesh grid size of

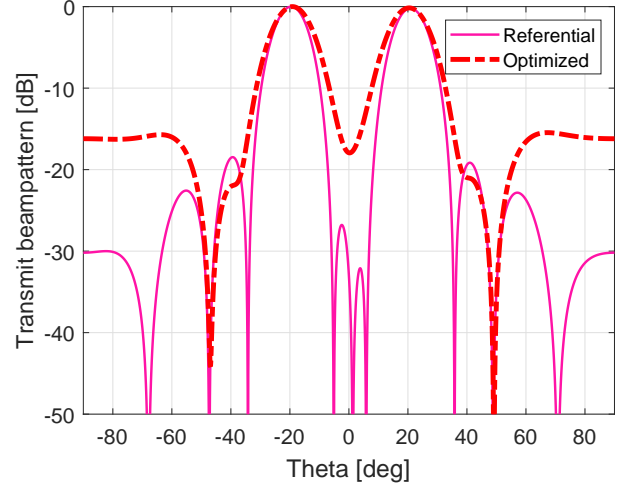


Fig. 9. Comparison between the optimized transmit beampattern and the reference transmit beampattern (multiple targets).

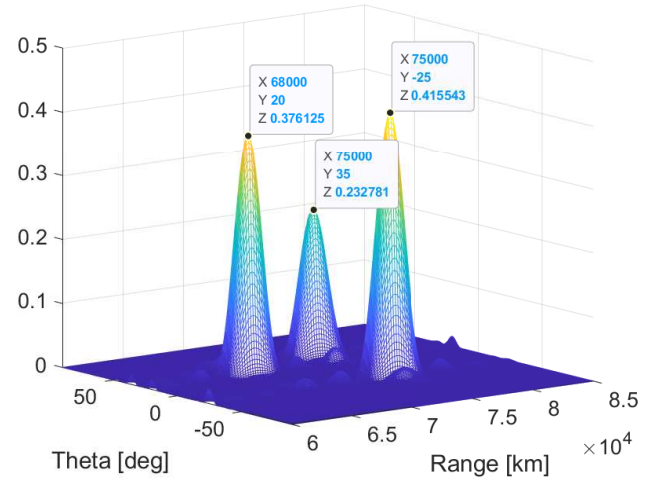


Fig. 10. 3-D transmit-receive beampattern.

$(0.1^\circ, 0.1 \text{ km})$. The three targets are located at $(-25^\circ, 75 \text{ km})$, $(20^\circ, 68 \text{ km})$ and $(25^\circ, 75 \text{ km})$. Fig. 9 compares the optimized transmit beampattern with the reference transmit beampattern.

In fact, range-related steering vector and angle steering vector are coupled in coherent FDA system. As previously analyzed, this coupling shown in the transmit beampattern is the widened mainlobe and the increased sidelobe. In particular, the joint transmit-receive design is configured in this paper. More specificity, receive weight vector mainly controls the focusing of echo energy. Transmit weight vector not only considers the energy allocation at the transmit end, but also needs to cooperate with the receive weight vector to realize the focusing of echo energy. The performance loss of the transmit beampattern is inevitable, but the output energy is optimal in system receiver end.

Fig.10 shows the output energy distribution at the coherent FDA receiver end. Fig. 11 and Fig. 12 draws the transmit-receive beampattern profile cut at the range and angle dimen-

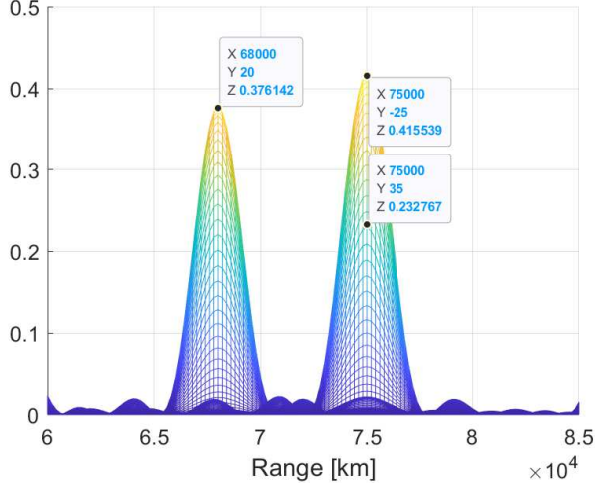


Fig. 11. Range profile of the transmit-receive beampattern.

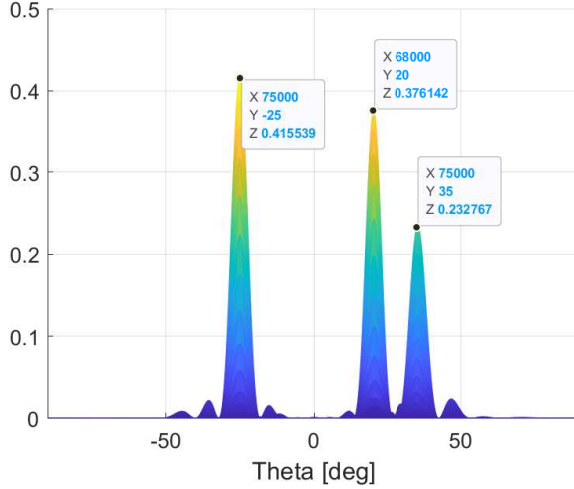


Fig. 12. Angle profile of the transmit-receive beampattern.

sions, respectively.

It is noted that the coherent FDA can also achieve energy focusing with low sidelobe for different targets in the same range. Therefore, the FDA enjoys the advantages of range-dependent beamforming, which provides a potential solution to suppress range-dependent interferences.

V. CONCLUSION

In this paper, we proved that the multi-carrier mixing receiver can retain the range information in the received FDA returns and systematically reformulated the FDA transceiver model with time-range relationship consideration, which is verified as the optimality in maximum likelihood estimation sense. More importantly, we devised a optimal design scheme of the joint transmit and receive weighting vectors to maximize the energy radiated within the interested two-dimensional range-angle sections for a given radiated energy. In order to tackle the resultant optimization problem, an iterative algorithm based on the SDR and randomization techniques is

proposed to obtain approximate solutions with good accuracy. All proposed methods are verified by theoretical analysis and numerical results. Note that possible future research might concern the further integration of baseband waveform design with the proposed array optimization for enhanced FDA radar performance.

APPENDIX A

Problem P_1 can be equivalently recast as the following QCQP optimization problem:

$$\begin{aligned} \min_{\mathbf{w}} \quad & \mathbf{w}^H \Omega_s \mathbf{w} \\ \text{s.t.} \quad & \mathbf{w}^H \Omega_t \mathbf{w} = 1 \end{aligned} \quad (66)$$

Consequently, the Lagrange function of above problem can be easily expressed as

$$L(\mathbf{w}, v) = \mathbf{w}^H \Omega_s \mathbf{w} + v \cdot (\mathbf{w}^H \Omega_t \mathbf{w} - 1) \quad (67)$$

where v denotes the Lagrange multiplier. Then, it follows from the Karush-Kuhn-Tucker (KKT) conditions that [32]

$$\begin{cases} \frac{\partial L(\mathbf{w}, v)}{\partial \mathbf{w}} = 2\Omega_s \mathbf{w}^* + 2v \cdot \Omega_t \mathbf{w}^* = 0 \\ v \geq 0 \end{cases} \quad (68)$$

Therefore, we have

$$\begin{aligned} (\mathbf{w}^*)^H \Omega_s \mathbf{w}^* + v \cdot (\mathbf{w}^*)^H \Omega_t \mathbf{w}^* &= 0 \Rightarrow (\mathbf{w}^*)^H \Omega_s \mathbf{w}^* = -v; \\ \Omega_s^{-1} \Omega_t \mathbf{w}^* &= -\frac{1}{v} \cdot \mathbf{w}^*. \end{aligned} \quad (69)$$

Note that

- 1) minimizing $\mathbf{w}^H \Omega_s \mathbf{w}$ is equivalent to minimizing $-v$;
- 2) \mathbf{w}^* is the eigenvector of matrix $\Omega_s^{-1} \Omega_t$, and the corresponding eigenvalue is $-\frac{1}{v}$.

As a result, we can infer that the optimal reference weight vector \mathbf{w}^* is the eigenvector corresponding to the maximum eigenvalue of matrix $\Omega_s^{-1} \Omega_t$. This completes the proof.

REFERENCES

- [1] J. Li and P. Stoica, *MIMO radar signal processing*. John Wiley & Sons, 2008.
- [2] J. Li, P. Stoica, L. Xu, and W. Roberts, "On parameter identifiability of mimo radar," *IEEE Signal Processing Letters*, vol. 14, no. 12, pp. 968–971, 2007.
- [3] L. Xu, J. Li, and P. Stoica, "Target detection and parameter estimation for mimo radar systems," *IEEE Transactions on Aerospace and Electronic Systems*, vol. 44, no. 3, pp. 927–939, 2008.
- [4] P. Antonik, M. C. Wicks, H. D. Griffiths, and C. J. Baker, "Multi-mission multi-mode waveform diversity," in *2006 IEEE Conference on Radar*. IEEE, 2006, pp. 3–pp.
- [5] W.-Q. Wang, H. C. So, and A. Farina, "An overview on time/frequency modulated array processing," *IEEE Journal of Selected Topics in Signal Processing*, vol. 11, no. 2, pp. 228–246, 2016.
- [6] W.-Q. Wang, "Ultrawideband frequency-diverse array antennas: Range-dependent and autoscanning beampattern applications," *IEEE Antennas and Propagation Magazine*, vol. 60, no. 3, pp. 48–56, 2018.
- [7] A. Basit, W.-Q. Wang, S. Wali, and S. Y. Nusenu, "Transmit beamspace design for fda-mimo radar with alternating direction method of multipliers," *Signal Processing*, vol. 180, p. 107832, 2021.
- [8] W.-Q. Wang, "Cognitive frequency diverse array radar with situational awareness," *IET Radar, Sonar & Navigation*, vol. 10, no. 2, pp. 359–369, 2016.
- [9] J. Xu, G. Liao, Y. Zhang, H. Ji, and L. Huang, "An adaptive range-angle-doppler processing approach for fda-mimo radar using three-dimensional localization," *IEEE Journal of Selected Topics in Signal Processing*, vol. 11, no. 2, pp. 309–320, 2016.

- [10] R. Gui and W.-Q. Wang, "Adaptive transmit power allocation for fda radar with spectral interference avoidance," in *2020 IEEE Radar Conference (RadarConf20)*. IEEE, 2020, pp. 1–6.
- [11] L. Wang, W.-Q. Wang, H. Guan, and S. Zhang, "Lpi property of fda transmitted signal," *IEEE Transactions on Aerospace and Electronic Systems*, 2021.
- [12] R. Gui, W.-Q. Wang, C. Cui, and H. C. So, "Coherent pulsed-fda radar receiver design with time-variance consideration: Sinr and crb analysis," *IEEE Transactions on Signal Processing*, vol. 66, no. 1, pp. 200–214, 2017.
- [13] Y. Xu, X. Shi, W. Li, J. Xu, and L. Huang, "Low-sidelobe range-angle beamforming with fda using multiple parameter optimization," *IEEE Transactions on Aerospace and Electronic Systems*, vol. 55, no. 5, pp. 2214–2225, 2018.
- [14] Y. Xu and K.-M. Luk, "Enhanced transmit–receive beamforming for frequency diverse array," *IEEE Transactions on Antennas and Propagation*, vol. 68, no. 7, pp. 5344–5352, 2020.
- [15] Y. Xu, X. Shi, J. Xu, and P. Li, "Range-angle-dependent beamforming of pulsed frequency diverse array," *IEEE Transactions on Antennas and Propagation*, vol. 63, no. 7, pp. 3262–3267, 2015.
- [16] J. Xiong, W.-Q. Wang, H. Shao, and H. Chen, "Frequency diverse array transmit beampattern optimization with genetic algorithm," *IEEE Antennas and Wireless Propagation Letters*, vol. 16, pp. 469–472, 2016.
- [17] L. Lan, J. Xu, G. Liao, Y. Zhang, F. Fioranelli, and H. C. So, "Suppression of mainbeam deceptive jammer with fda-mimo radar," *IEEE Transactions on Vehicular Technology*, vol. 69, no. 10, pp. 11 584–11 598, 2020.
- [18] J. Xu, S. Zhu, and G. Liao, "Range ambiguous clutter suppression for airborne fda-stap radar," *IEEE Journal of Selected Topics in Signal Processing*, vol. 9, no. 8, pp. 1620–1631, 2015.
- [19] W.-Q. Wang and H. Shao, "Range-angle localization of targets by a double-pulse frequency diverse array radar," *IEEE Journal of Selected Topics in Signal Processing*, vol. 8, no. 1, pp. 106–114, 2013.
- [20] S. M. Kay, *Fundamentals of statistical signal processing: estimation theory*. Prentice-Hall, Inc., 1993.
- [21] P. Antonik, M. C. Wicks, H. D. Griffiths, and C. J. Baker, "Frequency diverse array radars," in *2006 IEEE Conference on Radar*. IEEE, 2006, pp. 3–pp.
- [22] W.-Q. Wang, "Range-angle dependent transmit beampattern synthesis for linear frequency diverse arrays," *IEEE transactions on antennas and propagation*, vol. 61, no. 8, pp. 4073–4081, 2013.
- [23] M. A. Richards, *Fundamentals of radar signal processing*. McGraw-Hill Education, 2014.
- [24] M. I. Skolnik, *Radar handbook*. McGraw-Hill Education, 2008.
- [25] H. L. Van Trees, *Optimum array processing: Part IV of detection, estimation, and modulation theory*. John Wiley & Sons, 2004.
- [26] J. Xu, G. Liao, S. Zhu, L. Huang, and H. C. So, "Joint range and angle estimation using mimo radar with frequency diverse array," *IEEE Transactions on Signal Processing*, vol. 63, no. 13, pp. 3396–3410, 2015.
- [27] G. Cui, H. Li, and M. Rangaswamy, "Mimo radar waveform design with constant modulus and similarity constraints," *IEEE Transactions on signal processing*, vol. 62, no. 2, pp. 343–353, 2013.
- [28] Z. Cheng, Z. He, B. Liao, and M. Fang, "Mimo radar waveform design with papr and similarity constraints," *IEEE Transactions on Signal Processing*, vol. 66, no. 4, pp. 968–981, 2017.
- [29] O. Aldayel, V. Monga, and M. Rangaswamy, "Successive qcqp refinement for mimo radar waveform design under practical constraints," *IEEE Transactions on Signal Processing*, vol. 64, no. 14, pp. 3760–3774, 2016.
- [30] A. De Maio, Y. Huang, M. Piezzo, S. Zhang, and A. Farina, "Design of optimized radar codes with a peak to average power ratio constraint," *IEEE Transactions on Signal Processing*, vol. 59, no. 6, pp. 2683–2697, 2011.
- [31] A. Aubry, V. Carotenuto, and A. De Maio, "Forcing multiple spectral compatibility constraints in radar waveforms," *IEEE Signal Processing Letters*, vol. 23, no. 4, pp. 483–487, 2016.
- [32] S. Boyd, S. P. Boyd, and L. Vandenberghe, *Convex optimization*. Cambridge university press, 2004.
- [33] Z.-Q. Luo, W.-K. Ma, A. M.-C. So, Y. Ye, and S. Zhang, "Semidefinite relaxation of quadratic optimization problems," *IEEE Signal Processing Magazine*, vol. 27, no. 3, pp. 20–34, 2010.
- [34] M. Grant and S. Boyd, "Cvx: Matlab software for disciplined convex programming, version 2.1," 2014.
- [35] Z.-Q. Luo, T.-H. Chang, D. Palomar, and Y. Eldar, "Sdp relaxation of homogeneous quadratic optimization: approximation," *Convex Optimization in Signal Processing and Communications*, p. 117, 2010.